CILAMCE 2017
Florianópolis - Santa Catarina - Brazil

METHODS FOR ASTRONOMICAL IMAGE RESTORATION

Ana Paula A. C. Shiguemori

Murilo S. Dantas

anapaula.acs@ifsp.edu.br

murilodantas06@gmail.com

Instituto Federal de Educação Ciência e Tecnologia (IFSP)

Rua Antnio Fogaa de Almeida, 200, Zip: 12322-030, Jacareí, SP, Brazil

Elcio H. Shiguemori

elciohs@gmail.com

Departamento de Ciência e Tecnologia Aeroespacial (DCTA)

Av. Brigadeiro Faria Lima 1941, Zip: 12227-000, São José dos Campos, SP, Brazil

Alice Kozakevicius

Vinicius Monego

alice.kozakevicius@gmail.com

monego@mail.ufsm.br

Universidade Federal de Santa Maria (UFSM)

Av. Roraima, 1000 - Camobi, Zip: 97105-900, Santa Maria, RS, Brazil

Renata S. R. Ruiz

Cristiano Strieder

Haroldo F. Campos Velho

rennaruiz@gmail.com

cstrieder@gmail.com

haroldo.camposvelho@inpe.br

Instituto Nacional de Pesquisas Espaciais (INPE)

Av. dos Astronautas 1758, Zip: 12227-010, São José dos Campos, SP, Brazil

Abstract. *Image restoration is a kind of inverse problem of great relevance. It is one of the most important topics in image processing on space applications and astronomy. Remote sensing and autonomous navigation by images are typical requests. The focus of this paper is the evaluation of different restoration techniques based on truncated singular value decomposition, Tikhonov regularization method, neural network restoration, and wavelet filtering. The image restoration techniques are applied on astronomical images of planets of the solar system and from solar activity. Comparisons among the results are discussed.*

Keywords: *Astronomical images, Image restoration, Inverse problem*

1 INTRODUCTION

The process of image reconstruction or mitigation of degradation effects has motivated a great amount of research on this very important topic, which has many applications in science and technology: material science, medical tomography, biology, remote sensing, geophysics, autonomous navigation, and robotics are some examples. Image restoration can also be considered as a classical example of an inverse problem, belonging to the class of ill-posed problems. Our focus is driven to the astronomical image restoration.

A set of factors implies in the image degradation process, such as the distortion by the optical system, motion blur, light absorption during photon traveling, to mention a few. Several methods for image restoration has been developed. There is a large literature on the subject, one example is Beterro and Boccacci's book (1998), in which different methods are described. In this paper, our main goal is to contribute to the discussion in this field, increasing the comparison spectrum and analyzing the performances of more recent methodologies. In this sense, we apply four different methodologies to image restoration: Truncated Singular Value Decomposition (TSVD), regularized inverse solutions, wavelet shrinkage, and a new approach based on neural network (Castro et al., 2008) – in which multiscale data is the novelty for the training process. The performance of the four different approaches is evaluated considering an image from a solar loop and a degraded image of the Saturn planet. Noisy synthetic images are produced, allowing the comparison between the original and the reconstructed images.

Our motivation to study different methods for astronomical image restoration is linked to a project developed by the National Institute for Space Research (INPE: Instituto Nacional de Pesquisas Espaciais), Brazil: the Brazilian Deimetric Array (BDA) – see: BDA web-page. Two methodologies are well established, TSVD and Tikhonov regularization, and other two are relatively recent, wavelet and multiscale neural network, opening a new range of possibilities to be further investigated.

The paper is organized as follows. Section 2 describes the restoration methods considered for the analysis. Section 3 presents results for the astronomical degraded images, considering different metrics as figures of merit. Finally, Section 4 addresses the conclusions.

2 IMAGE RESTORATION TECHNIQUES

Digital image is a matrix L, in which the coordinates (x, y) and the light intensity $L(x, y)$ (brightness) are discrete values (Gonzalez and Woods, 1992). The space coordinates (x, y) are represented by row and column entries of L and are the addresses of *pixels*, the smallest controllable element of a picture represented on a display device. Therefore the matrix values $L(x, y)$ are the gray levels (from white to black) per pixel (per position). A color image is a composition of three images, one in red, one in green and the other in blue (RGB) color, with different intensity levels for each pixel.

During the transmission or image acquisition process, a kind of image degradation is usually associated. When noise is present in the image, we are dealing with a degraded image. Image degradation can compromise interpretation and even important information can be lost. In some applications, image processing is essential to carry out a particular action.

Some image restoration techniques will be described in this section and applied later on test images. Here, the restoration process is applied to a gray degraded image.

2.1 Truncated singular value decomposition (TSVD)

Truncated singular value decomposition (TSVD) is a special form of the singular value decomposition (SVD) in which the computation is limited. This limitation can lead to interesting performance characteristics.

The singular value decomposition refers to the factorization of a real or complex matrix. It is the generalization of the eigendecomposition (representation of a matrix in terms of eigenvalues and eigenvectors) to any $m \times n$ matrix via an extension of the polar decomposition. It has many useful applications in signal processing and statistics.

Formally, the singular value decomposition of an $m \times n$ real or complex matrix $\mathbf{M}$ is expressed as:

$$\mathbf{M} = \mathbf{U}\mathbf{\Sigma}\mathbf{V}^*, \tag{1}$$

being $\mathbf{U}$ an $m \times m$ real or complex unitary matrix. $\mathbf{\Sigma}$ is a $m \times n$ rectangular diagonal matrix with non-negative real numbers on the diagonal and $\mathbf{V}$ is an $n \times n$ real or complex unitary matrix. The superscript "*" denotes conjugate transposed matrix. The diagonal entries σ_i of $\mathbf{\Sigma}$ are known as the singular values of $\mathbf{M}$. The columns of $\mathbf{U}$ and the columns of $\mathbf{V}$ are called the left-singular vectors and right-singular vectors of $\mathbf{M}$, respectively.

In the TSVD form, only t column vectors of $\mathbf{U}$ and t row vectors of $\mathbf{V}^*$, corresponding to the t largest singular values σ_t, are calculated. The rest of the matrix is discarded. This can be much quicker and more economical if $t \ll r$, being r the rank of matrix $\mathbf{M}$. The matrix $\mathbf{U}_t$ is thus $m \times t$, $\mathbf{\Sigma}_t$ is $t \times t$ diagonal, and $\mathbf{V}_t^*$ is $t \times n$. The TSVD is no longer an exact decomposition of the original matrix $\mathbf{M}$, instead it is expressed as

$$\tilde{\mathbf{M}} = \mathbf{U_t}\mathbf{\Sigma_t}\mathbf{V_t^*}, \tag{2}$$

in which the approximated $\tilde{\mathbf{M}}$ is in very useful sense the closest approximation to $\mathbf{M}$ that can be achieved by a matrix of rank t.

The Truncated SVD form pertains to a class named Reduced SVD. Other formulations are the Thin SVD and the Compact SVD (Golub and Van Loan, 1996). For many applications, it might be sufficient (as well as faster and less demanding in storage) to compute a reduced version of the SVD procedure.

2.2 Tikhonov regularization

Typically, for (inverse) ill-posed problems, existence, uniqueness and stability of their solutions cannot be ensured. In some sense, a solution can be formulated in such a way that existence and uniqueness can be relaxed, but this solution can still be unstable under the presence of noise in the experimental data. Hence, a solution determination requires some regularization technique, i.e., the incorporation in the inversion procedure of some available information about the true solution. Following the Tikhonov approach according to Tikhonov and Arsenin (1977), a regularized solution is obtained by choosing the function I^* that minimizes the following functional

$$M^\alpha \left[I^{\mathrm{ref}}, I\right] = \|I - I^{\mathrm{ref}}\|_2^2 \, + \, \alpha\,\Omega[I], \tag{3}$$

in which I^{ref} is a reference image, $I = H\{I^{\mathrm{ref}}\}$ – being $H\{.\}$ the image acquisition system, $\Omega[I]$ denotes the regularization term, α is the regularization parameter, and $\|\cdot\|_2$ is the 2-norm.

The regularization parameter α is chosen numerically, assuming that a bound δ (or the 'statistics') of the measurement error is known, i.e., $||I_{\text{exact}} - I||_2 \leq \delta$. This numerical procedure is based on Morozov's discrepancy principle: α^* is chosen such that I_{α^*} minimizes Eq. (3) and

$$R(f_{\alpha^*}) := ||I_{\alpha^*} - I^{\text{ref}}||_2^2 = \delta^2,$$

i.e., the residual $R(I_{\alpha^*})$ and the bound on the measured data are the same.

A well-known regularization technique proposed by Tikhonov (Tikhonov and Arsenin, 1977) can be expressed by

$$\Omega[I] = \sum_{k=0}^{p} \alpha_k \left\| I^{(k)} \right\|_2^2, \tag{4}$$

in which $I^{(k)}$ denotes the k-th derivative relative to (x, y), since $I = I(x, y)$, and the regularization parameters $\alpha_k \geq 0$. Here, if $\alpha_k = \delta_{kj}$ (Kronecker's delta), i.e.,

$$\Omega[f] = \left\| f^{(j)} \right\|_2^2,$$

then the method is called the *Tikhonov regularization of order j* (Tikhonov-j). Particularly, the Tikhonov regularization of order zero will be referenced only as *Tikhonov regularization*. Following the previous terminology, we observe that the effect of the Tikhonov regularization ($\Omega[f] = ||I||_2^2$) is to filter out the oscillations on the restored image: *smooth* function $I(x, y)$. On the other hand, the Tikhonov regularization of first order makes $|\partial I/\partial x + \partial I/\partial y| \approx 0$, that is, $I(x, y)$ is approximately constant.

Clearly, as $\alpha_k \to 0$ the least squares term in the objective function is over-estimated, what might not give good results in presence of noise (Tikhonov and Arsenin, 1977). On the other hand, if $\alpha_k \to \infty$, all consistency with the information about the system is lost.

2.3 Wavelet restoration

Wavelet thresholding is a well established technique used for data denoising, filtering, restoration, and compression, applied in various research areas assuming continuous or discrete, uni- or multidimensional data affected by different types of noise or perturbations (Hashemi and Beheshti, 2014).

Generally presenting, wavelet thresholding methods are based on two main steps: the wavelet decomposition done for a chosen wavelet transform and the analysis of the wavelet coefficients generated by the transformation. The most common used type of dyadic wavelet decomposition consists of decomposing the signal into two half subbands of low and high frequency called, respectively, scaling (means) and wavelet (details) coefficients. Given that an image is a two-dimensional signal, each dimension is decomposed into two halves, giving four subbands in the first decomposition level, one containing the scaling coefficients and the other three containing wavelet coefficients of different nature, usually identified as horizontal, vertical and diagonal, according to the chosen algorithm for realizing the 2D transform (Stollnitz and DeRose, 1995). If more decomposition levels are necessary, only the scaling subband is further decomposed. In this work, the orthonormal family of Daubechies wavelets is considered for the transformation, assuming periodic data extension on the boundaries.

The image denoising process based on the wavelet decomposition exploits the property that most of the noise lies on the wavelet coefficients associated to high frequencies, i.e. those obtained in the initial levels. With that in mind, the second step of the analysis consists in selecting a threshold value and compare it to the wavelet coefficients. One simple strategy to discard non-significant (noisy) components of the data is to set to zero all wavelet coefficients below the threshold value, while data above this threshold will be preserved (hard threshold) or shrinked (soft threshold) – see Donoho and Johnstone (1994).

The optimal choice of the threshold value is the one that maximizes the elimination of noise and minimizes the elimination of the signal. After the threshold operation is applied, the signal is then reconstructed by the inverse wavelet transform, outputting the denoised image.

Several strategies, usually called *thresholding methods*, exist to estimate the optimal threshold value, for a more detailed discussion see (Kozakevicius and Bayer, 2014). In the current work, two of the most common and widely used methods are tested, the VisuShrink (Donoho and Johnstone, 1994) and the BayesShrink (Chang et al., 1997).

VisuShrink

VisuShrink applies a single threshold value, called the *universal threshold*, to all the detail subbands for all decomposition levels obtained by the wavelet decomposition. Assuming σ the standard deviation of the diagonal details and N is the image's pixel count, its value is given by:

$$UT = \sigma\sqrt{2\log N}\ . \tag{5}$$

The universal threshold value is generally large and tends to kill a fair amount of relevant components of the signal along with the noise. Another issue is the consideration of the same threshold value independently of the decomposition level of the transform, which might become disproportional and incoherent with respect to the magnitude of the wavelet coefficients in the coarsest levels of the decomposition. As a consequence, the reconstructed image is oversmoothed.

BayesShrink

As observed, the choice of a single threshold on all subbands might not be the best strategy because it basically relies on the noise information of only one subband, discarding the magnitude variations that might occur because of the scale variations throughout the wavelet decomposition. Methods that consider different threshold values computed based on the analyzed data are called adaptive. A comparison among different adaptive methods for 1D data is done by Bayer and Kozakevicius (2010). In this work, the well established BayesShrink is considered. It is an adaptive method that improves the denoising process by taking into account specific information to each subband, assigning threshold values adaptively.

In the work Hashemi and Beheshti (2014), these threshold values were modeled for a range of noise variance σ_w, signal variance $\sigma_{\bar{y}}$, and shape parameter β. Based on that, a closed form representation that best describes the BayesShrink threshold as a function of these three parameters (σ_w,$\sigma_{\bar{y}}$,β) was obtained.

In Hashemi and Beheshti (2014) it was also shown that the Bayes estimator for general Gaussian distributed signals. The *Bayes estimator* behaves very much like a soft thresholding algorithm. The BayesShrink scheme searches for the optimum soft threshold that minimizes the MSE error and maps the observation to a class of threshold values in the form of $(\sigma_w)^{c_1}(\sigma_{\bar{y}})^{c_2}$, assuming the shape parameter β as being 1. One widely used option for the BayesShrink threshold value per level is setting $c_1 = 2$ and $c_2 = -1$.

2.4 Artificial neural network (ANN)

The Artificial Neural Network techniques have been employed with success in several image processing applications. The main classes of applications are those that need some type of information processing in real time. This characteristic is desired when it is necessary to process a large amount of data in the shortest time in a specific hardware. The ANN activation have a low computational cost, which makes it suitable for signal analysis applications, among them astronomical image restoration.

There are different methods based on artificial neural networks. Castro et al. (2008) have presented a new multiscale method for training a neural network designed for image restoration. The training data are selected by sampling a set of pixels from co-centered disks with different gray levels – see Figure 1a for noisy image (left) and noiseless image (right).

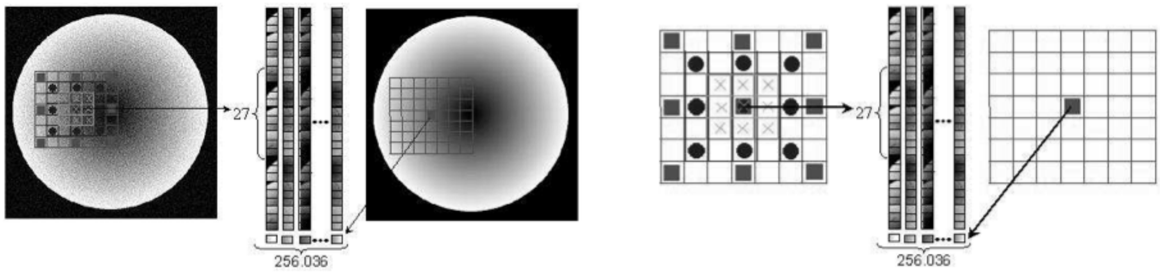

(a) (b)

Figure 1: Multyiscale: (a) *linearization* from concentric circles with different gray levels: noisy (left) and noiseless (right) images, (b) subsample method using the 7x7 window neighborhood.

Three windows with 3x3, 5x5, 7x7 from the noisy image and the corresponding window center position in the original noiseless image were used to establish the training set. Subsamples from the 5x5 and 7x7 windows were employed to form two 3x3 windows to simulate the multiscale formulation. The gathering from three 3x3 windows data created the input vector for learning process. The desired target for the learning phase was the the pixel in the center of the corresponding 7x7 window in the noiseless image (Castro et al., 2008). The mentioned procedure produced a very large training data set. In order to reduce the amount of data for the learning phase, a data mining scheme was applied based on a Kohonen neural network.

For the data mining process, a similarity Gaussian metric was employed. During the Kohonen neural neural training procedure, a competition among neurons is carried out, where a threshold limit is applied. The winning neuron had to overcome the threshold (robustness) to have its weight updated. If the winner neuron did not overcome this threshold, a new neuron had to be inserted in the one-dimensional lattice to represent the input vector whose elements were assigned to the corresponding elements of the weight vector see Figure 2. Two similarity thresholds were used: a 0.9 and 0.8 of a Gaussian transformation of the distance of the weight vector of each neuron to the input vector (Castro et al., 2008).

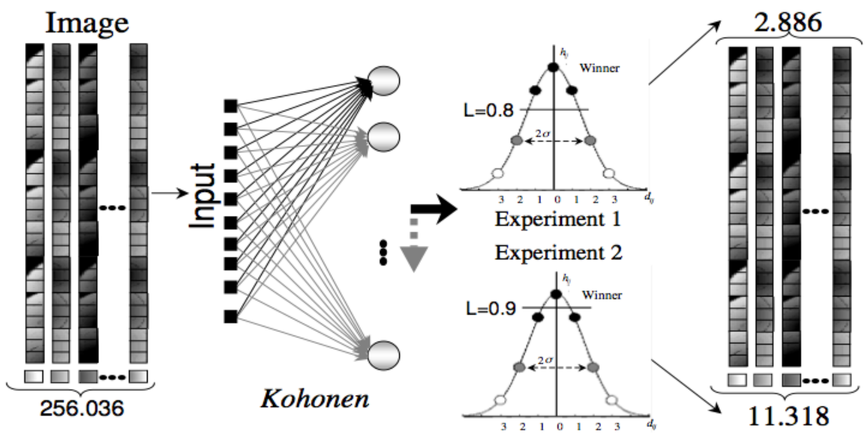

Figure 2: Data mining by cluster anlysis using Kohonen neural network.

3 RESULTS

Two astronomical images are used for testing the restoration techniques presented in the previous sections: a solar loop snapshot, and Saturn planet – see Figures 3a and 4a. The synthetic observed images are obtained by adding a Gaussian white noise:

$$I(x, y) = h(x, y) * \hat{I}(x, y) + \tau(x, y), \tag{6}$$

in which $I(x, y)$ is the image to be restored, $\hat{I}(x, y)$ is the original image and $h(x, y)$ is the acquisition system (camera). The operator ”*” represents the convolution, and $\tau(x, y)$ denotes the noise. Noiseless and noisy images for a solar loop and the Saturn planet are shown in Figures 3 and 4, respectively.

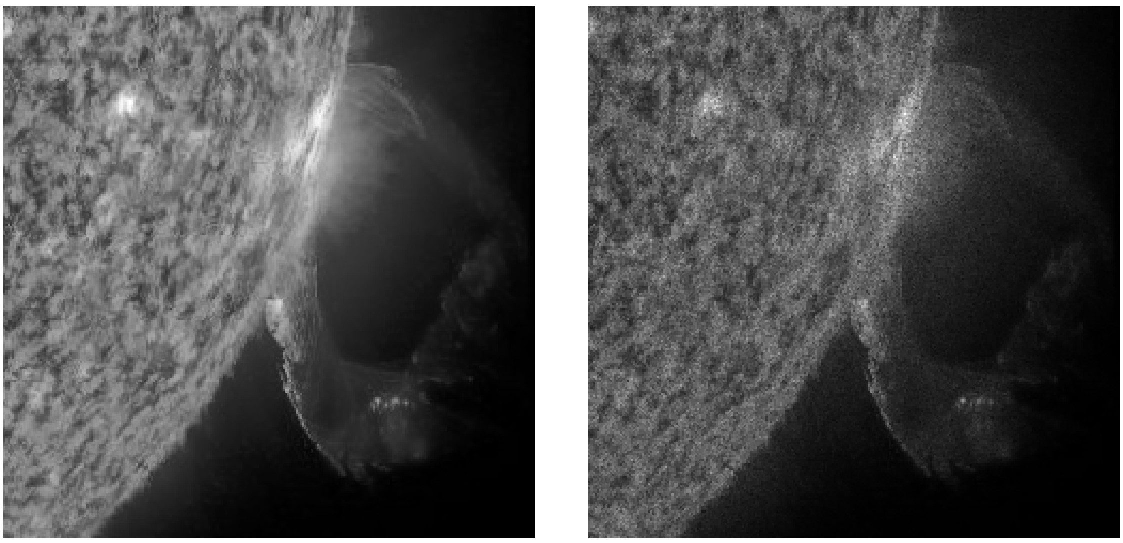

(a) (b)

Figure 3: Solar loop images: (a) original, (b) noisy.

The image acquisition system $h(x, y)$ (see Eq. 6) is simulated by a Point Spread Function (PSF). The PSF is modeled by a Gaussian function $N_{\mathrm{PSF}}(\mu, \sigma)$. For our tests, the PSF was

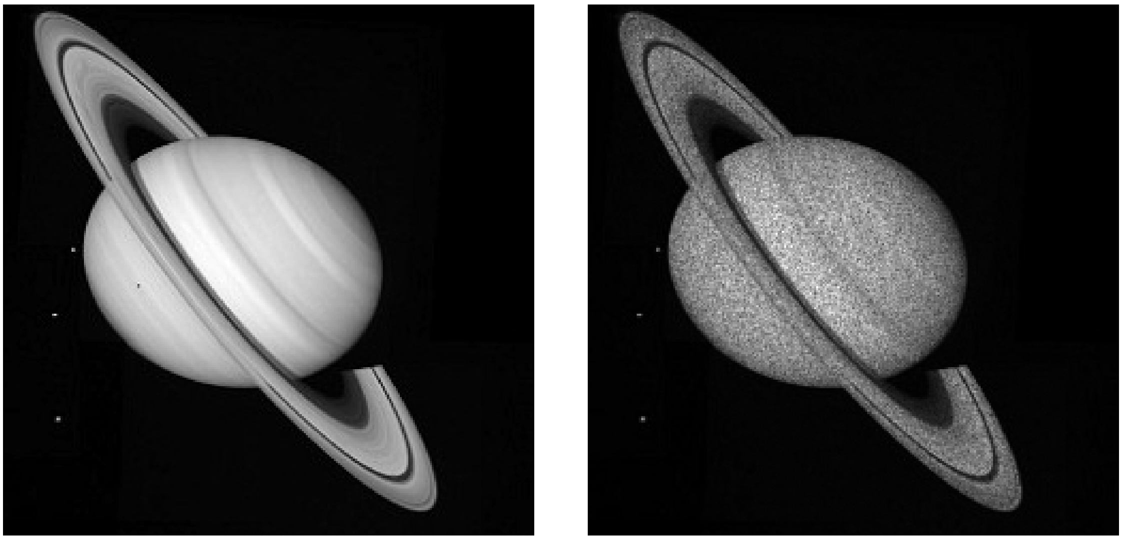

(a) (b)

Figure 4: Saturn planet images: (a) original, (b) noisy.

considered $N_{\mathrm{PSF}}(0, 0.4)$. The noise is assumed to be represented by a a Gaussian distribution with zero mean and standard deviation equal to 0.15: $\tau = N_{\mathrm{noise}}(0, 0.15)$.

3.1 Restoration: TSVD and Tikhonov regularization

The dimension of both images is 249×249, resulting 249 singular values for a complete decomposition. The restoration by applying the TSVD was performed by the Morosov's discrepancy principle. For the solar loop denoising, only 31 singular values were used for restoring the image. The Saturn planet image restoration was obtained with 27 singular values in the truncated version of the SVD algorithm. The restored images are displayed in Figures 5a and 6a for solar loop and Saturn planet, respectively.

Three orders of Tikhonov regularization operators were employed. Figures 5b, 5c, and 5d show the solar loop restoration by Tikhonov zeroth, first and second orders. The image restoration for Saturn planet using the cited three orders of Tikhonov regularization is shown in Figures 6b, 6c, and 6d. The Morosov's discrepancy principle was also employed to find the regularization parameters for each order of Tikhonov regularization. The regularization parameters are shown in Table 1. The E04UCF routine from the NAG numerical library (1993) was used for solving the minimization problem – see Section 2.2, Eq. (3). This routine is designed to minimize an arbitrary smooth function subjected to constraints (simple bounds, linear and nonlinear constraints), using a sequential programming method, codifying quasi-Newton approximation to the Hessian matrix.

3.2 Restoration: Wavelets

For performing the wavelet shrinkage, the considered function is the `denoise_wavelet` provided by the scikit-image project (Van der Walt et al., 2014), which is a collection of image processing algorithms in Python, version 0.14dev.

This function supports both methods mentioned above (as part of version v0.14) and requires four parameters: the wavelet type, the threshold mode, levels of decomposition and the

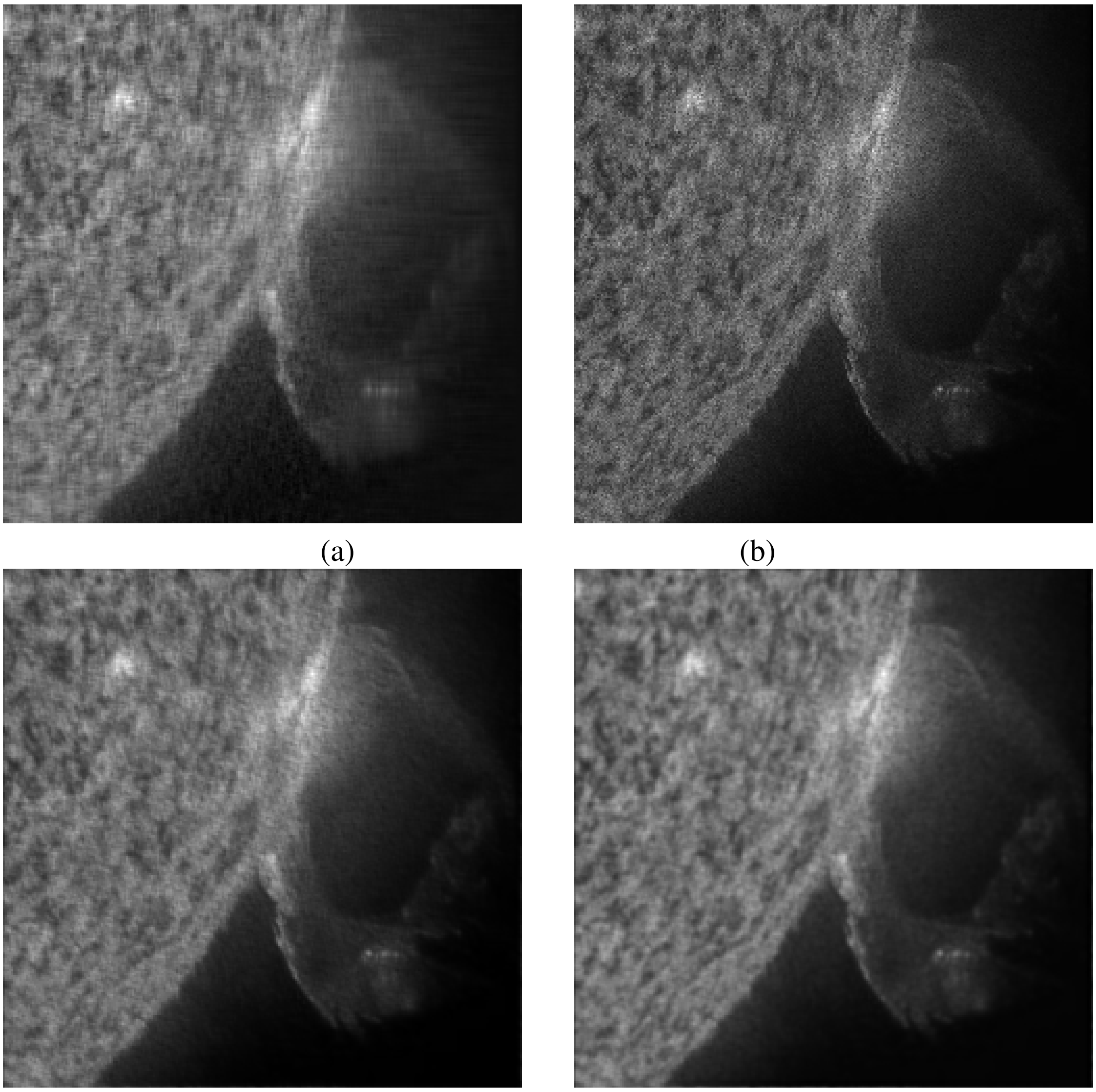

(c) (d)

Figure 5: Solar loop image restoration by TSVD and Tikhonov regularization: (a) TSVD, (b) Tikhonov zeroth order, (c) Tikhonov first order, (d) Tikhonov second order.

standard deviation. The defaults were used for the performed tests, which are the db1 (Haar) wavelet, soft threshold mode and three less than the maximum number of possible decomposition levels. For an image of size 256×256, four decomposition levels are possible, minus three means that only the first level of decomposition is used. Here, the simplest option for the wavelet basis is chosen, associated to a smoothing strategy for the shrinkage of the wavelet coefficients. We point out that different combinations of the possible choices for each one of the parameters can generate different filtering results. In fact, the application in quest is a decisive factor in setting up all parameters.

The noise standard deviation, the fourth parameter to be informed, is estimated by the method proposed in (Donoho and Johnstone, 1994), considering MAD the median absolute

Table 1: Regularization parameter computed from the Morosov's discrepancy principle.

Image	Tikhonov-0	Tikhonov-1	Tikhonov-2
Solar Loop	0.4701	0.5763	0.4763
Saturn planet	0.5254	0.6641	0.5254

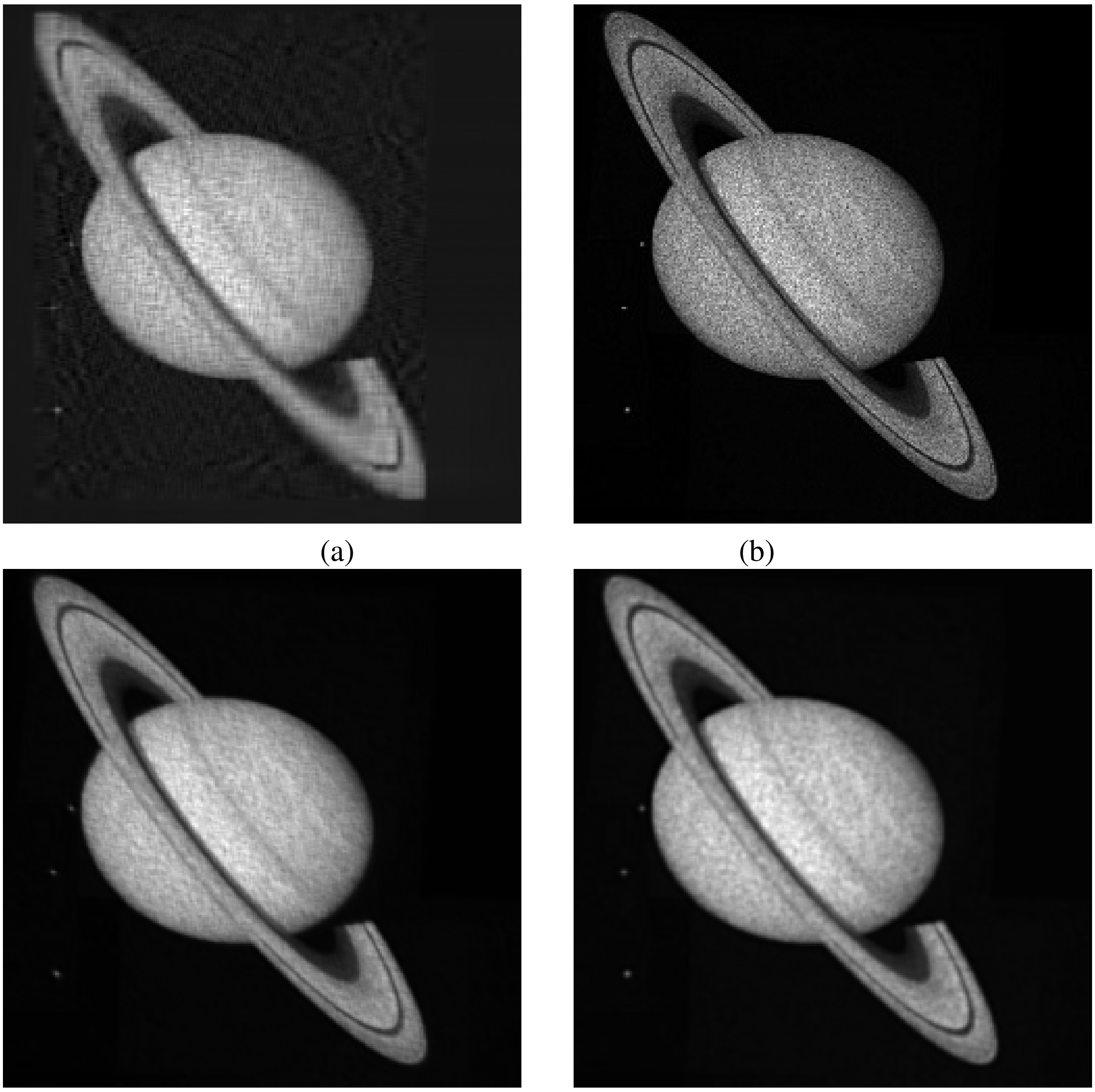

(a) (b) (c) (d)

Figure 6: Saturn image restoration by TSVD and Tikhonov regularization: (a) TSVD, (b) Tikhonov zeroth order, (c) Tikhonov first order, (d) Tikhonov second order.

deviation and ppf(0.75) as being the 75^{th} percentile of the noise distribution:

$$\sigma = \frac{MAD}{ppf(0.75)} \ . \tag{7}$$

A disadvantage worth mentioning of working with standard algorithms for performing dyadic wavelet transforms is the necessity of assuming that the signal dimension is given as a power of two. Otherwise, the algorithms have to be modified or the signal dimension has to adjusted, imposing any type of extension or restriction of the data. Since in our test cases the images were of dimensions 249×249, the signal had to be extended. The strategy used was symmetric extension, that is, the last row and column are duplicated until the image dimension becomes 256×256 . Requiring signal extension will have a negative, although small, impact in the denoising process because unoriginal data had to be introduced and accounted for. Kozakevicius and Schmidt (2013) did a discussion about data extrapolation and a simplified treatment given for the boundaries in a wavelet transform is presented.

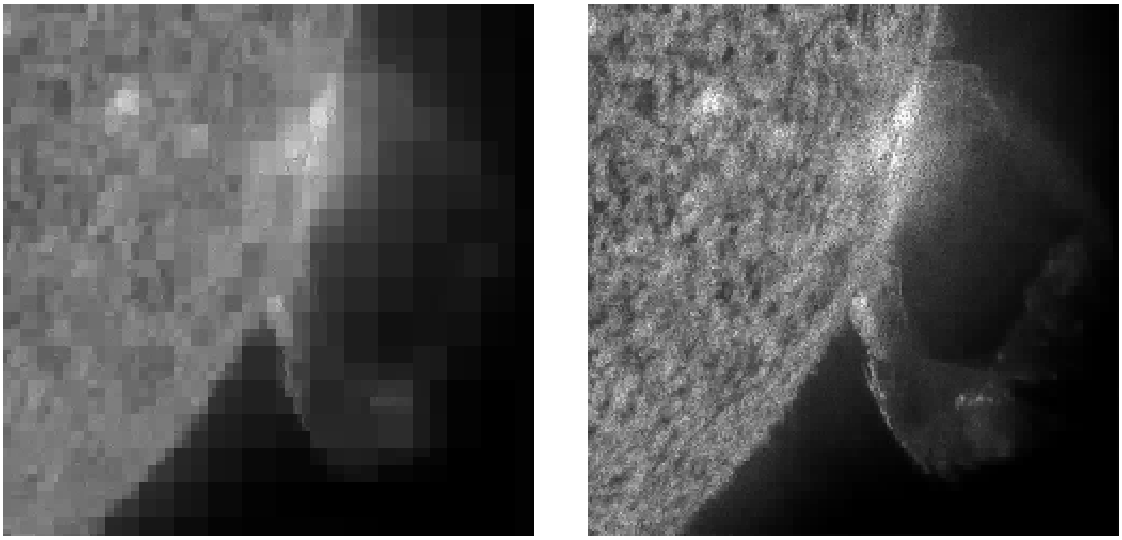

(a) (b)

Figure 7: Solar loop by wavelet restoration – approaches: (a) VisuShrink, (b) BayesShrink.

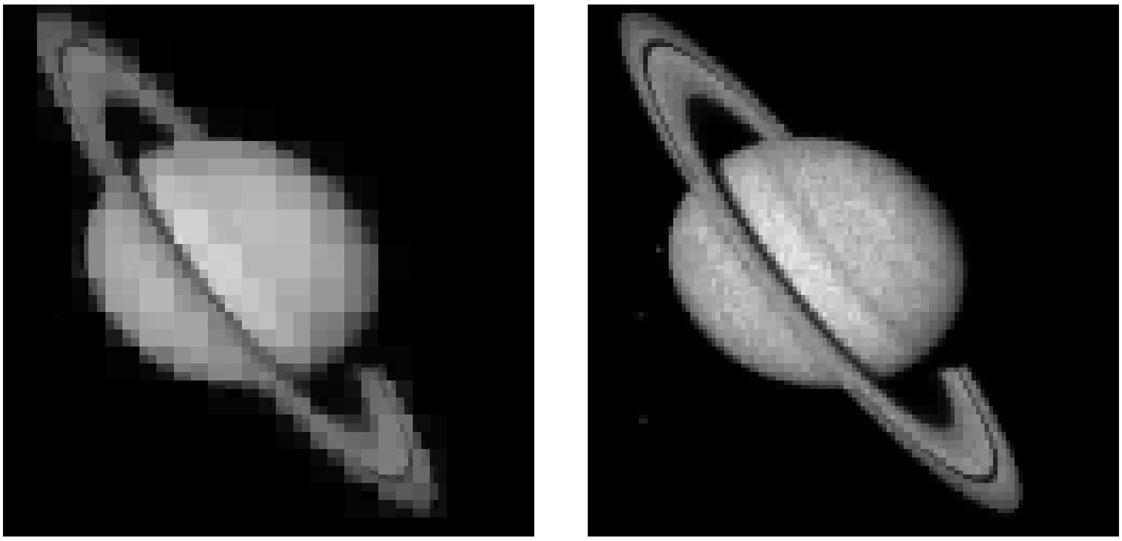

(a) (b)

Figure 8: Saturn by wavelet restoration – approaches: (a) VisuShrink, (b) BayesShrink.

3.3 Restoration: Artificial Neural Network

The multiscale approach applying neural network is tested for the solar loop and Saturn images. The learning process was performed with the noisy image as input to the multilayer perceptron (MLP) and the noiseless image data as the target output. The MLP was designed with 1 hidden layer with 14 neurons, and logistic sigmoidal activation function was applied in each neuron. Several training parameters were considered.

The restoration process with multiscale neural network is shown in Figure 9a, for solar loop, and Figure 9b, for Saturn planet image. A good performance for restoration was also noted from the degraded images.

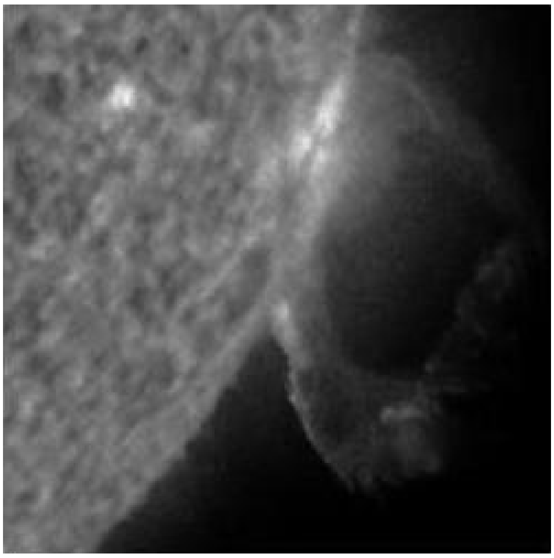

(a)

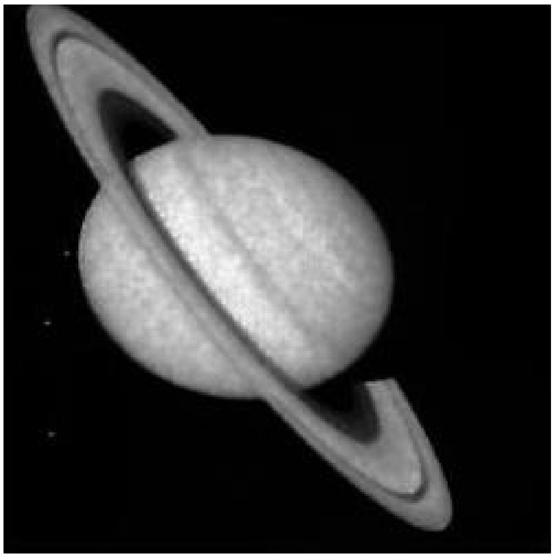

(b)

Figure 9: Images restoration by neural multiscale filter: (a) solar loop, (b) Saturn.

3.4 Restoration evaluation

Section 2 did a brief description of image restoration techniques used in this paper. Results for 2 astronomical images, considering different restoration methods, are presented in Section 3. Here, a quantitative comparison is done, performing an evaluation for the applied restoration schemes. Five parameters are employed to do a comparative evaluation: average, variance, RMS (*Root Mean Square*), entropy, and SNR (*Signal-Noise Ratio*). The original and noisy images should have similar numerical values to the average and variance. Therefore, the restored images must also present similar behavior. The entropy indicates the image smoothness. The restoration process should present the closer entropy value with the value computed from the original image. The entropy is calculated by the expression:

$$S = -\sum_i \sum_j p_{ij} \log p_{ij} \ . \qquad (8)$$

in which the p_{ij} is the pixel intensity for the image.

Table 2 presents a quantitative performance for Solar loop image, where Wave-1 and Wave-2 denote the wavelets restoration using VisuShrink and BayesShrink approaches, respectively.

Table 2: Solar loop: quantitative comparison among image restoration techniques.

L. Solar	Original	Deg.	Tik-0	Tik-1	Tik-2	TSVD	Wave-1	Wave-2	NN
Mean	75.73	75.76	62.05	75.76	75.76	75.77	75.67	75.65	??
Variance	123.90	120.34	116.46	126.29	125.45	124.65	133.20	122.96	??
RMS	-	11.76	19.69	7.65	7.35	9.64	12.01	11.08	??
Entropy	7.24	7.34	7.08	7.24	7.23	7.27	6.90	7.23	??
SNR	-	-	-4.48	3.74	4.08	1.73	0.25	1.01	??

Table 3: Saturn planet: quantitative comparison among image restoration techniques.

Saturn	Original	Deg.	Tik-0	Tik-1	Tik-2	TSVD	Wave-1	Wave-2	NN
Mean	39.17	39.18	30.71	39.18	39.18	39.16	39.06	39.05	??
Variance	71.12	71.17	70.52	72.08	72.09	72.36	71.96	70.22	??
RMS	-	9.20	17.36	5.44	5.66	8.81	14.01	9.17	??
Entropy	4.90	5.03	4.73	4.96	4.93	5.32	3.91	3.55	??
SNR	-	-	-5.52	4.57	4.22	0.38	-0.58	1.64	??

The acronimum “NN” represents restoration by multiscale neural network. Methods applying Tikhonov-1 and Tikhonov-2 formulations presented the lowest values for the RMS. Table 3 showed the evaluations for Saturn planet restoration. The regularized inverse Tikhonov solutions of higher orders also showed the better values for the RMS.

4 CONCLUSION

Image restoration has strong importance of many applications in science and technology. In particular, astronomy and astrophysics deal with optical telescopes, radiotelescopes, and radio-interferometric telescopes, among other probes. One central issue of these instruments is the analysis from images. The Brazilian Deimetric Array (BDA) is a radio-interferometric instrument, in which image restoration is one of research topics (Sawant et al., 2000). The goal of the current work was to provide an evaluation of standard and modern methodologies for image denoising to be applied in the BDA project.

Four different restoration techniques were presented and applied to two astronomical images: TSVD, Tikhonov regularized inversion, wavelet restoration, and multiscale neural network. For the worked astronomical images, the results indicated that the restoration with Tikhonov-1 and Tikhonov-2 presented better performances. However, these methods demand a higher computational cost than other ones.

ACKNOWLEDGEMENTS

Authors want to thank the Brazilian agencies for research support: FAPERGS, FAPESP, CNPq, and CAPES.

REFERENCES

Bertero, M., & P. Boccacci, 1998. *Introduction to Inverse Problems in Imaging*, Institute of Physics London.

A. P. A. Castro, I. N. Drummond, J. D. S. Silva, 2008. A multiscale neural network method for image restoration. TEMA (Tend. Mat. Apl. Comput.), vol. 9, No. 1, pp. 41-50.

Gonzalez,R. C., & Woods, R. C., 1992. *Digital Image Processing*, Addison Wesley.

BDA (Brazilian Decimetric Array): `http://www.das.inpe.br/fmi/bda/`

Golub, G. H., Van Loan, C. F. (1996). *Matrix Computations* (3rd ed.). Johns Hopkins.

Tikhonov, A. N., & Arsenin, V.Y., 1977. *Solutions of Ill-Posed Problems*, Winston and Sons.

Hashemi, M., & Beheshti, S., 2014. Adaptive Bayesian Denoising for General Gaussian Distributed Signals. *IEEE Transactions on Signal Processing*, vol. 62, n. 5, pp. 1147-1156.

Stollnitz, E. J., & DeRose, A. D., 1995. Wavelets for computer graphics: a primer-1, *IEEE Computer Graphics and Applications*, vol. 15, n. 3, pp. 76 -84.

Donoho, D. L., & and Iain M. Johnstone, I. M., 1994, Ideal spatial adaptation by wavelet shrinkage. *Biometrika*, vol. 81, pp. 425-455.

Chang, S. G., Yu, B., & Martin Vetterli, M., 2000, Adaptive Wavelet Thresholding for Image Denoising and Compression. *IEEE transactions on image processing* , vol.9, n.9, pp.1532-1546.

Kozakevicius, A., & Bayer, F. M., 2014. Signal denoising via wavelet coefficients thresholding. *Ciência e Natura* (edição especial 35 anos), vol.36, pp. 37-51 ,

F. M. Bayer, F. M., & Kozakevicius, A. J., 2010. SPC-Threshold: uma proposta de limiarizao para filtragem adaptativa de Sinais. *TEMA*, vol. 11, n. 2, pp. 121-132.

Van der Walt, S., Schönberger, J. L., Nunez-Iglesias, J., Boulogne, F. , Warner, J. D., Yager, N., Gouillart, E., Yu, T., & scikit-image contributors, 2014, Scikit-image: image processing in Python. *PeerJ*, pp. e453 (available in: `http://dx.doi.org/10.7717/peerj.453`).

Kozakevicius, A., & Schmidt, A. A., 2013. Wavelet transform with special boundary treatment for 1D data. *Computational and Applied Mathematics*, vol. 32, n. 3, pp. 447457.

E04UCF, 1993. *NAG Fortran Library Mark 13*, Oxford, UK.

Sawant, H. S., Subramanian, K. R., Ldke, E., Sobral, J. H. A., Swarup, G., Fernandes, F. C. R., Rosa, R. R., & Cecatto, J. R., 2000. Brazilian Decimetric Array. *Advances in Space Research*, vol. 25, No. 9, pp. 1809-1812.